BIOCHEMISTRY
including biophysical chemistry & molecular biology

Article

pubs.acs.org/biochemistry

Binding Efficiency of Protein−Protein Complexes

Eric S. Day,[†] Shaun M. Cote,[‡] and Adrian Whitty*[,‡]

[†]Biogen Idec, 14 Cambridge Center, Cambridge, Massachusetts 02142, United States

[‡]Department of Chemistry, Boston University, Boston, Massachusetts 02215, United States

Supporting Information

ABSTRACT: We examine the relationship between binding affinity and interface size for reversible protein−protein interactions (PPIs), using cytokines from the tumor necrosis factor (TNF) superfamily and their receptors as a test case. Using surface plasmon resonance, we measured single-site binding affinities for binding of the large receptor TNFR1 to its ligands TNFα (K_D = 1.4 ± 0.4 nM) and lymphotoxin-α (K_D = 50 ± 10 nM), and also for binding of the small receptor Fn14 to TWEAK (K_D = 70 ± 10 nM). We additionally assembled data for all other TNF−TNFR family complexes for which reliable single-site binding affinities have been reported. We used these values to calculate the binding efficiencies, defined as binding energy per square angstrom of surface area buried at the contact interface, for nine of these complexes for which cocrystal structures are available, and compared the results to those for a set of 144 protein−protein complexes with published affinities. The results show that the most efficient PPI complexes generate ∼20 cal mol^{-1} Å^{-2} of binding energy. A minimal contact area of ∼500 Å^2 is required for a stable complex, required to generate sufficient interaction energy to pay the entropic cost of colocalizing two proteins from 1 M solution. The most compact and efficient TNF−TNFR complex was the BAFF−BR3 complex, which achieved ∼80% of the maximal achievable binding efficiency. Other small receptors also gave high binding efficiencies, while the larger receptors generated only 44−49% of this limit despite interacting primarily through just a single small domain. The results provide new insight into how much binding energy can be generated by a PPI interface of a given size, and establish a quantitative method for predicting how large a natural or engineered contact interface must be to achieve a given level of binding affinity.

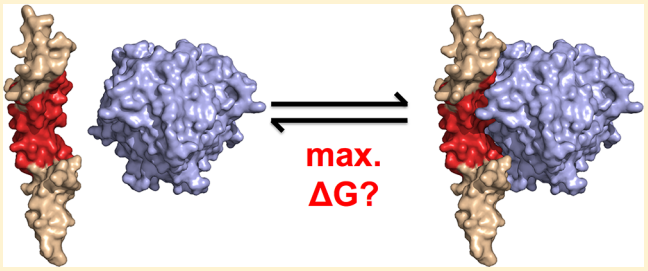

Understanding the molecular origins and the magnitudes of protein−protein binding energies is critical to achieving a quantitative picture of biological function at the molecular level. This knowledge is also important for the development of drugs for modulating such functions and for designing engineered proteins to achieve desired binding properties. In 1999, Kuntz and co-workers attempted to quantify the maximal binding affinity that a protein can achieve with a small molecule ligand of a given size.[1] They showed that relatively small ligands (those containing up to ∼10 non-hydrogen atoms) can generate as much as ∼1.5 kcal/mol of binding energy per heavy atom of their structure through interactions with their target protein. This seminal publication led to the development of the important concept of ligand efficiency, the assessment of binding strength in terms of binding energy divided by the number of heavy atoms in a ligand's structure,[2] as a means to quantify how effectively a given small ligand or set of atoms within a ligand interact with a protein to generate binding affinity. The concept of ligand efficiency has become important in drug discovery, where minimizing the size of the ligand (drug) is often critical to achieving good pharmaceutical properties,[3] and is now widely used to evaluate the quality of screening hits and to guide drug lead optimization. The aim of this study is to extend the concept of ligand efficiency to protein−protein interactions (PPIs) by determining the maximal binding efficiency, i.e. binding affinity per unit contact area, that can be achieved for interaction with a protein ligand of a given size, and how the binding efficiencies observed for a set of structurally homologous PPI complexes, involving tumor necrosis factor (TNF) family ligands binding to their cognate TNFR family receptors, compare to this maximal value.

For small molecule ligands, the number of heavy atoms is a simple and convenient surrogate for molecular size. For protein−protein interactions, on the other hand, the total number of heavy atoms in a participating protein is essentially irrelevant to binding affinity, as the majority of atoms do not directly participate in binding. Nor is the number of heavy atoms actually involved at the binding interface a particularly convenient measure of interface size. Therefore, the ligand efficiency of a PPI complex is best described in terms of binding energy per square angstrom of interface area. For the purpose of this study, we call this quantity "binding efficiency" (units of calories per mole per square angstrom), to distinguish it from the established term "ligand efficiency" with its specific meaning of binding energy per heavy atom (or, sometimes, per unit of molecular weight) of the ligand.[2]

Received: August 1, 2012
Revised: October 19, 2012
Published: October 22, 2012

   dx.doi.org/10.1021/bi301039t | *Biochemistry* 2012, 51, 9124−9136

Cytokines of the tumor necrosis factor (TNF) superfamily and their receptors provide a good case study for examining variations in the affinities that can be achieved for reversible protein−protein interactions with binding interfaces of different sizes. TNF family cytokines are constitutive trimers that contain three receptor binding sites, one at each subunit interface of the ligand (Figure 1A). TNF family receptors possess a modular structure in their extracellular region, containing one or several cysteine rich domains (CRDs), each CRD itself comprising a pair of modules with conserved disulfide bonding patterns (Figure 1B).[4] The first ligand−receptor cocrystal structure reported for this family, lymphotoxin-α (LTα, also known as TNFβ or TNFSF1) bound to the extracellular portion of TNF receptor 1 (TNFR1, also known as TNFRp55 or TNFRSF1A) which contains four CRDs, revealed that each trimeric ligand binds three TNFR1 molecules to form a 3-fold symmetric complex, with each receptor forming an extensive contact surface primarily involving its second and third CRDs (Figure 1A).[5] Other TNFR superfamily members with multiple CRDs adopt a similar binding geometry with their respective ligands.[6−14] In recent years, however, a number of TNFRs that are much smaller than the prototypical TNFR1 have been discovered.[15] Some of these contain only a single CRD or, in the case of BR3 (BAFFR, TNFRSF13C), just a fragment of a CRD.[16] X-ray and NMR structures of small TNFRs bound to their cognate TNF family ligands show that they conform to the same basic binding topology established for the larger receptors but occupy only a fraction of the binding footprint defined by TNFR1 with LTα (Figure 1C).[17−19] TNF−TNFR family interactions thus constitute a set of homologous protein−protein complexes that display a range of interface sizes within an overall binding mode that is quite conserved.

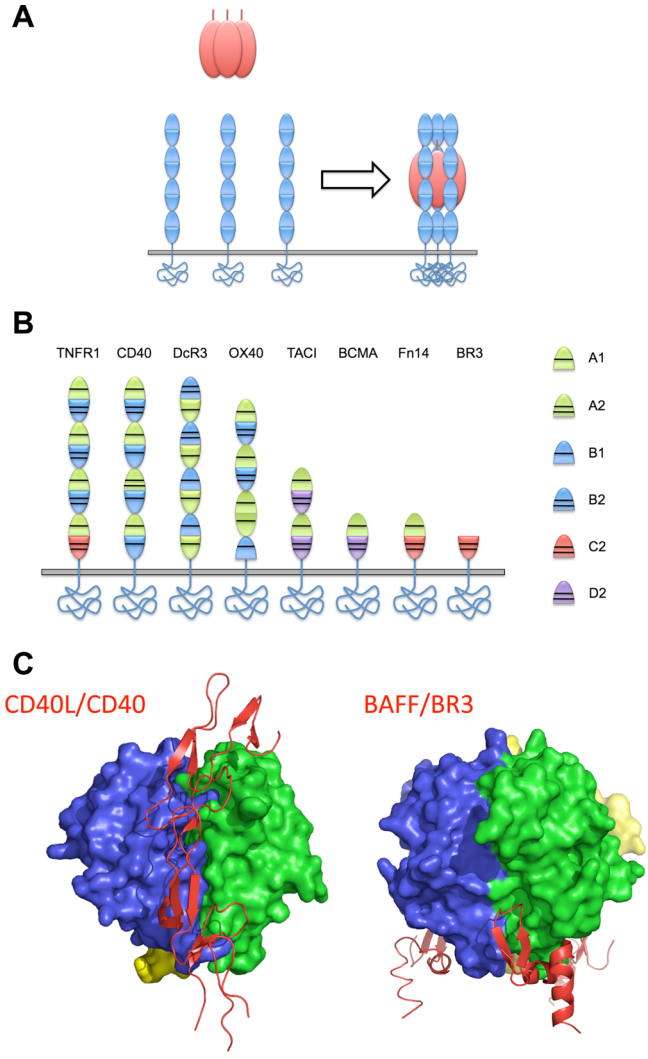

Figure 1. Structure and mode of interaction of TNF superfamily ligands with their receptors. (A) Cartoon illustrating how a trimeric TNF family ligand binds to three TNFR family receptor molecules to form a 1:3 complex, with the TNFR molecules binding in the clefts at the subunit interfaces on the ligand. (B) Modular structure of the eight TNFR family receptors considered in this study. The receptors contain up to four cysteine-rich domains (CRDs), each comprising a pair of modules designated by a letter (A, B, C, or D) to indicate the fold and a number (1 or 2) corresponding to the number of disulfides present. The receptors considered in this study vary in size from TNFR1, CD40, and DcR3, each of which contains four CRDs, to BR3, which contains only one-half of a CRD. (C) X-ray cocrystal structures of CD40−CD40L (PDB entry 3QD6) and BR3−BAFF (PDB entry 1OQE) complexes, showing that the overall binding mode is conserved but BR3 occupies a much smaller portion of the binding groove on the ligand.

We recently reported single-site binding affinities of two of the smaller TNFR receptors, BR3 and BCMA, for their cognate ligands BAFF and APRIL.[20] By separating affinity from avidity effects, we were able to gain new insights into the selectivity of BAFF and APRIL for their preferred receptors versus other receptors that they can also bind. Somewhat to our surprise, we found that these small receptors bind with high affinity, comparable to or in some cases much greater than the single-site affinities we observed for some much larger TNF ligand−receptor pairs such as the CD40L−CD40 pair[21] in which the receptors contain up to four CRDs and appear to have more extensive binding interfaces (Figure 1C). Thus, within the TNF−TNFR superfamilies, different receptor−ligand pairs appear to manifest a wide range of values for the amount of binding energy they generate per unit of contact surface area.

The relationship between binding energy and interface size for PPI complexes has been addressed in previous studies, using a range of approaches.[22−26] Some publications report overall trends between binding affinity and the amount of surface area buried at the interface, typically quantified as the change in solvent-accessible surface area (ΔASA), for particular data sets.[22−24,26−29] However, in general, there is agreement that PPI complexes develop under a variety of evolutionary constraints, such as stability, solubility, and selectivity, that in many cases will trump any evolutionary pressure to maximize interaction affinity. Thus, across a diverse set of PPI complexes, no strong correlation between ΔG_0 and ΔASA is expected or observed.[22,23,27] The question of what is the maximal amount of binding energy that can be achieved for a PPI with a given interface size has not been definitively answered, however. Brooijmans et al. have proposed that very small PPIs can generate up to 1.5 kcal/mol of binding energy per non-hydrogen ligand atom at the interface,[22] but this conclusion required a rather long, nonlinear extrapolation from a set of PPI complexes, all of which had actual measured binding efficiencies ranging from ~0.07 to ~0.31 kcal/mol per non-hydrogen interface atom.

This study focuses specifically on what available experimental data reveal about the maximal binding efficiencies that can be achieved by proteins engaging in reversible PPI or, at least, the highest efficiencies that are actually achieved in real systems.

dx.doi.org/10.1021/bi301039t | *Biochemistry* 2012, 51, 9124−9136

The goal is to gain insight into the physicochemical and structural factors that limit the amount of binding energy that proteins can generate through their interactions with other proteins. To address this question, we report a systematic analysis of single-site receptor−ligand binding affinities across a set of TNF−TNFR complexes that includes both larger and smaller binding interfaces, and calculate the amount of binding energy per unit of contact area that is achieved by each. To place the binding efficiency of the TNF−TNFR complexes on a scale relative to the maximal achievable binding efficiency for a reversible protein−protein interaction, we perform a similar analysis for a set of 144 protein−protein complexes using published affinity values, and use these results to propose a maximal binding efficiency (i.e., binding energy per square angstrom of contact area) that is observed for reversible protein−protein complexes. In addition to shedding light on ligand−receptor recognition in the TNF−TNFR family, the results provide new insight into how much binding energy can be generated by a PPI interface of a given size, and suggest a minimal value for how extensive a natural or engineered PPI contact interface must be to achieve a given level of binding affinity.

MATERIALS AND METHODS

Proteins and Reagents. Recombinant soluble human TWEAK was purified as previously described.[30] Briefly, a construct encoding human TWEAK residues A106−H249 was expressed in *Pichia pastoris*. The fermentation medium was concentrated and diafiltered and then purified by ion exchange on a Q Sepharose column, followed by a Zn chelating column, and finally by size exclusion chromotagraphy using a Sephacryl 300 column. LTα was purified from baculovirus-infected Sf9 (Life Technologies) insect cell culture medium produced as described previously.[31] Cells and cell debris were removed by centrifugation and filtration. The clarified insect cell supernatant containing LTα was concentrated by ultrafiltration and purified using a TNF-R55-Fc affinity column prepared as described previously.[31] TNFα was expressed and purified as previously described.[32] Briefly, the protein was expressed in *Escherichia coli* and purified using tandem HiTrap S HP columns, followed by tandem HiTrap Q HP columns (Amersham). The protein was dialyzed against 10 mM Tris (pH 7.5), 50 mM NaCl, 1 mM β-ME, and 1 mM cysteamine at 4 °C overnight to complete native disulfide bond formation. β-ME and cysteamine were removed by dialysis against 10 mM Tris (pH 7.5) and 50 mM NaCl overnight at 4 °C. The solution was ultrafiltered before it was stored at −80 °C. The soluble TNFR1 extracellular domain was expressed and purified as described in ref 32. Briefly, a construct encoding the human TNFR1 extracellular domain, residues 40−201, was expressed in *E. coli* and purified from inclusion bodies by being denatured in 6 M guanidine hydrochloride, 100 mM Tris (pH 8.5), 4 mM PMSF, and 20 mM DTT. Oxidized glutathione (30 mM) was added, and the solution was slowly diluted 10-fold with 50 mM Tris (pH 10.7), 6 mM cysteine, and 4 mM PMSF and then incubated overnight while being gently stirred at 4 °C. Insoluble material was removed by centrifugation. The supernatant was dialyzed twice against 50 mM Tris (pH 7.5) at 4 °C and then twice again against 50 mM MES (pH 6.2) with 25 mM NaCl at 4 °C. Insoluble material was once again removed by centrifugation and subsequent passage through a 0.2 μm filter. The resulting protein solution was purified over an Uno-S column (Pharmacia), and the fractions containing TNFR1 were sterilized by 0.2 μm filtration before being stored. This protein was shown to be monomeric by sodium dodecyl sulfate−polyacrylamide gel electrophoresis (SDS−PAGE) (Figure S1 of the Supporting Information) and was shown to be fully active by comparison with recombinant soluble TNFR1 from two other, independent sources; all three TNFR1 preparations showed identical affinities for binding to TNFα in a homogeneous time-resolved FRET competition assay measuring their ability to compete against XL665-labeled TNFR for binding to europium-labeled TNFα (J. Friedman et al., unpublished observations). The soluble Myc- plus His-tagged human Fn14 extracellular domain, residues 28−80, was purified and characterized as described previously.[33] Briefly, the protein was expressed in *P. pastoris* and purified by Ni/NTA affinity chromatography followed by size exclusion chromatography. The purified protein was characterized by mass spectrometry and was shown to be monomeric by SDS−PAGE and by gel filtration[33] (see representative SDS−PAGE data in Figure S1 of the Supporting Information). Proper folding of the recombinant Fn14 protein was established by showing that all cysteine residues in the protein were fully oxidized, by establishing the disulfide bond connectivity by proteolytic digestion followed by mass spectrometry, and by comparing its binding activity to that of Fn14 protein produced using other expression systems.[33]

Biacore Binding Measurements. *Biacore Chip Preparation.* All experiments were performed using a Biacore 3000 instrument (GE Healthcare). Soluble TNF family ligands were immobilized on CM5 sensor chips using the Biacore Amine Coupling Kit according to the manufacturer's instructions. Ligands were diluted in 10 mM acetate buffer and injected over Biacore sensor chip flow cells that had been activated with a 1:1 *N*-hydroxysuccinimide (NHS)/1-ethyl-3-[3-(dimethylamino)-propyl]carbodiimide hydrochloride (EDC) mixture. Excess free amine groups were then capped with a 50 μL injection of 1 M ethanolamine. The ligand surfaces were conditioned with 5 × 30 s injections of regeneration solution (see Table 1).

Table 1. Conditions Used To Prepare and Regenerate the Derivatized Biacore Sensor Chips Used in the Binding Experiments

	TWEAK	TNFα	LTα
ligand concentration (mg/mL)	50	75	50
pH of 10 mM acetate	5.0	5.5	6.5
NHS/EDC activation volume (μL)	50	5	5
ligand injection volume (μL)	50	5	5
typical immobilization level (RU)	1000−2000	∼300	∼1000
regeneration solution	10 mM H_3PO_4	50 mM glycine (pH 4.0) and 500 mM NaCl	50 mM glycine (pH 4.0) and 500 mM NaCl

A flow rate of 10 μL/min was used for all immobilization procedures. Exact conditions and typical immobilization levels for each ligand are listed in Table 1. For each experiment, underivatized control surfaces were prepared in the same manner as the ligand surface, except that acetate buffer containing no protein was injected in place of ligand. Biacore buffer [10 mM HEPES (pH 7), 150 mM NaCl, 3.4 mM EDTA,

and 0.005% p-20 detergent] was used as the running buffer during TWEAK immobilizations. The same buffer, except containing 0.0005% p-20 (low-detergent buffer), was used for TNFα and LTα immobilizations. The activity of the sensor chip surface generated by coupling the TNF family ligand was established by its ability to bind the appropriate receptor saturably and reproducibly and with high affinity. In each case, a number of different running buffers and regeneration conditions were tested, and the best condition was further optimized to find buffers that maintained the integrity of the trimeric TNF family ligands captured on the biosensor surface, while efficiently dissociating any bound receptor at the end of each cycle. Note that the running buffers that were used contained Tween 20 detergent and 0.05% BSA, to minimize the possibility that the soluble monomeric receptor proteins might form any weak, nonspecific aggregates that might affect their binding properties. The stability of each derivatized sensor chip surface and its robustness to repeated cycles of binding and regeneration were established in two ways: (i) by monitoring any progressive decrease in the magnitude of the baseline signal (i.e., the signal level observed after regeneration of the surface but before receptor is passed over the chip) resulting from disruption of the trimeric structure of the coupled TNF family ligand followed by dissociation of the released subunits and (ii) by testing for reproducibility in the receptor binding capacity of the surface, as measured by the amplitude of the binding signal observed when a given concentration of receptor was passed over the chip. After careful selection and optimization of the capture conditions, the running buffer, and the regeneration buffer, we were able to find for each TNF family ligand conditions that provided a stable surface that showed negligible degradation of its receptor binding capacity over multiple cycles of binding and regeneration.

TWEAK–Fn14 Kinetic Binding Assays. Soluble, monomeric human Fn14 was diluted in Biacore assay buffer (Biacore buffer with 0.05% BSA) to the indicated concentrations and injected over the TWEAK-derivatized surface, or over an underivatized (i.e., NHS/EDC-activated and then ethanolamine-capped) surface as a background control, at a flow rate of 50 μL/min. Following the injection of the protein, dissociation was monitored for 10 min at the same flow rate. The TWEAK surface was regenerated with 2 × 30 s injections of 10 mM H_3PO_4. In all cases, binding to the underivatized chip was negligible.

TNFα–TNFR1 and LTα–TNFR1 Kinetic Binding Assays. Soluble monomeric TNFR1 was diluted in low-detergent buffer [10 mM HEPES (pH 7), 150 mM NaCl, 3 mM EDTA, 0.05% BSA, and 0.0005% p-20] to the indicated concentrations and injected over the TNFα- or LTα-derivatized surfaces, or over underivatized surfaces as a background control, at a flow rate of 30 μL/min for approximately 8 min (250 μL injection volume). Receptor dissociation was then allowed to proceed for 15 min before surface regeneration by 2 × 30 s injections of 50 mM glycine (pH 4.0) and 500 mM NaCl. In all cases, binding to the underivatized chip was negligible.

Biacore Data Analysis. Prior to the fitting of the data, all sensorgrams were "double-referenced"; that is, each sensorgram was background-corrected by subtracting the data for the same solution run over the underivatized sensor surface and then subtracting the similarly treated data for the buffer alone (i.e., [TNFR] = 0) sample run on the ligand-derivatized surface. The binding affinity was determined by performing a global fit of the double-referenced sensorgrams from a given experiment to the kinetic model for simple, single-site binding shown below, using BIAevaluation:

$$dAB/dt = k_a AB - k_d AB$$

$$dB/dt = -(k_a AB - k_d AB)$$

where A = concentration, $B[0] = R_{max}$, and $AB[0] = 0$.

For the TWEAK–Fn14 and LTα–TNFR1 interactions, the equilibrium binding affinity was also determined by the alternative method of plotting the equilibrium response value seen at long association times (R_{eq}) versus receptor concentration [L] and fitting the data to the hyperbolic, single-site binding equation $R_{eq} = R_{max}[[L]/([L] + K_D)]$, where R_{max} represents the response at saturating receptor concentrations.

Calculation of Buried Surface Areas. The extent of the solvent-accessible surface area buried at the interface of each complex was calculated using PyMOL version 1.3, after first modifying the PDB files where necessary to generate the symmetry mates required to recapitulate the full ligand trimer bound to three receptor molecules. Waters and other solvent species were removed prior to the calculation. A probe of radius of 1.4 Å was used, and the "dot density" was set to 4. The surface area buried at the interface in each complex was calculated by subtracting the sum of the solvent-accessible surface areas for each protein component alone from that for the complex, and dividing the result by 3 to obtain the ΔASA per receptor interface. For complexes in which the unit cell contained multiple distinct complex geometries or in which two independent structures have been reported, the results for the observed ligand–receptor geometries were averaged. PyMol calculates ASA values by the method of Lee and Richards,[34] as does NACCESS,[35] which was used to calculate ΔASA values for the entries in the PPIA database.[27] To confirm that these two programs gave comparable results, we calculated ΔASA for one of the complexes using both methods and found the values to be in close agreement. Moreover, the complex of APRIL with TACI is also included in the PPIA database, and the ΔASA value reported for this complex agreed with the value we calculated here within ~1.5%. ΔASA values for individual CRDs were calculated by creating a separate object in PyMol for each CRD using the CRD boundaries for each receptor given by UniProt[36] and then subtracting ASA for the hypothetical ligand–CRD complex from that for the ligand with CRD alone. In some cases, the sum of the ΔASA values for the separate CRDs slightly exceeds the ΔASA value obtained for the full receptor, presumably because regions of the ligand that interact with the receptor close to the junction between adjacent CRDs are partially blocked from solvent by each CRD alone, as well as by the whole receptor, leading to some minor redundancy in the ΔASA calculations for the separate CRDs. Throughout this work, ΔASA refers to the total solvent-accessible surface area buried at the interface, including the surface on both the receptor and ligand sides of the interaction.

RESULTS

Despite the long history of biochemical study of TNF family cytokines and their receptors, until recently the literature contained surprisingly few values for the binding affinity of TNF receptor proteins for individual binding sites on TNF family ligands. Most published binding studies have used receptor proteins attached to a surface (e.g., cell membrane,

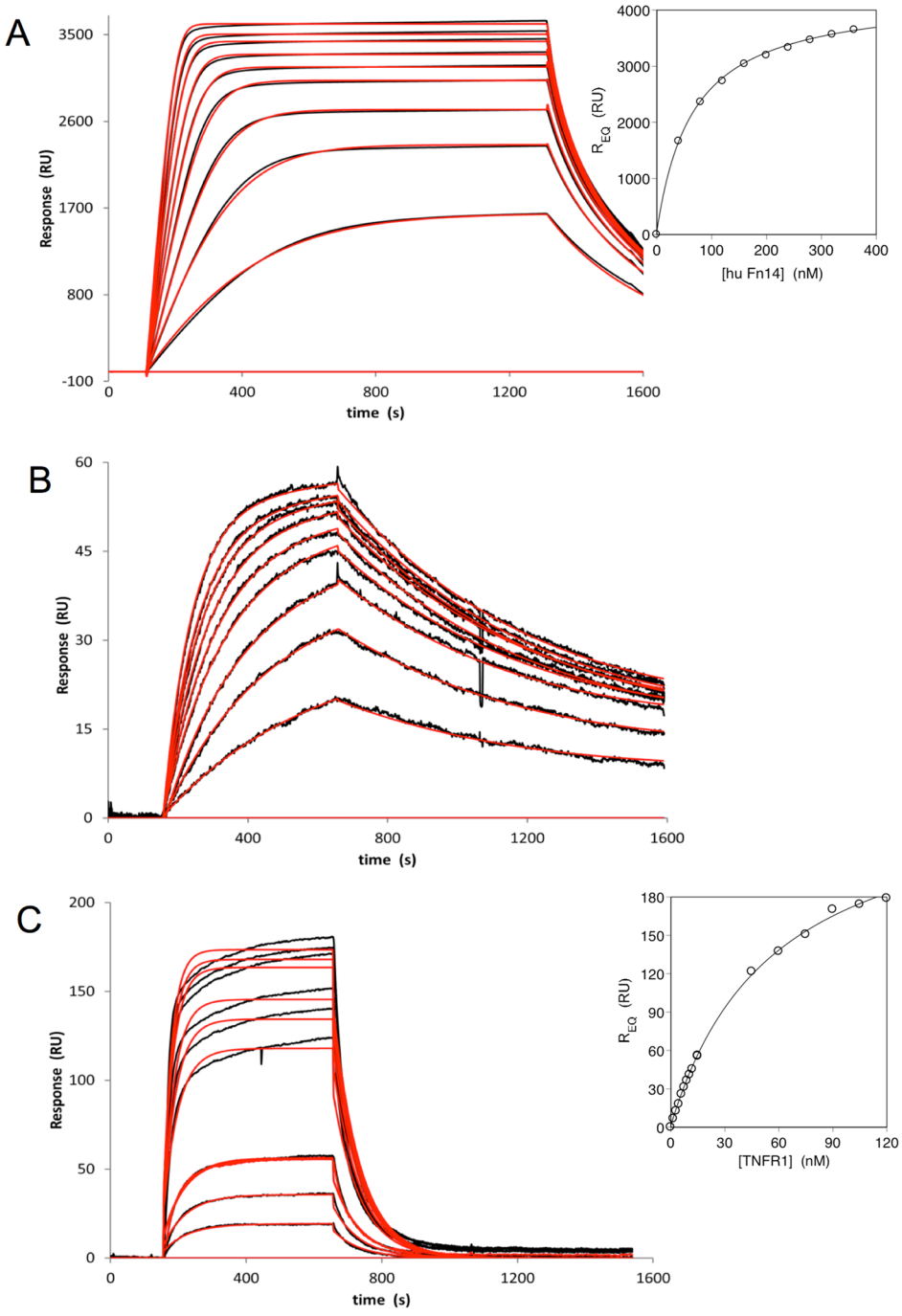

Figure 2. Biacore analysis of soluble monomeric receptors binding to TNF family ligands. Sensorgrams for (A) 40−360 nM soluble monomeric Fn14 binding to TWEAK, (B) 15−150 nM soluble monomeric TNFR1 binding to TNFα, and (C) 15−400 nM soluble monomeric TNFR1 binding to LTα on separate Biacore CM5 sensor chips. The experimental data (black lines) were globally fit to a 1:1 binding model (red lines) using BIAevaluation, as described in Materials and Methods, to determine kinetic rate constants. The insets in panels A and C show the signal observed at equilibrium, R_{eq}, plotted as a function of soluble receptor concentration, fit to a hyperbolic, single-site binding equation. Data are representative of at least three independent experiments.

assay plate, or sensor chip) or bivalent or multivalent receptor constructs, such that binding to the trimeric ligand is multivalent. Multivalent binding between TNF cytokines and their receptors reflects an important feature of how these proteins interact in vivo, but the apparent K_D values measured in such studies reflect both affinity and avidity effects and cannot be deconvoluted to determine an accurate number for the interaction energy associated with a single TNF−TNFR binding interface.

For this study, we supplemented the small number of existing single-site binding affinities with measurements for three additional TNF−TNFR family interactions for which we could find no published values in the literature. We chose complexes involving receptors at the high and low end of the size range for the TNFR superfamily: TNFR1, which contains four CRDs in its extracellular structure, binding to TNFα and also to its alternate ligand, LTα, and Fn14 that contains only one CRD (Figure 1B) binding to TWEAK. Binding affinities

dx.doi.org/10.1021/bi301039t | *Biochemistry* 2012, 51, 9124−9136

Table 2. Available Single-Site Binding Affinities and Binding Efficiencies of TNF−TNFR Family Complexes

ligand	receptor (no. of CRDs)	K_D (nM)	ΔG_0[a] (kcal/mol)	ΔASA[b] (Å^2)	binding efficiency (cal mol^{-1} Å^{-2}) apparent[c]	binding efficiency (cal mol^{-1} Å^{-2}) intrinsic[d]
TNFα	TNFR1 (4)	1.4 ± 0.4[e]	−12.1 ± 0.2	2524 ± 93	4.8 ± 0.2	8.8 ± 0.8
LTα		50 ± 10[e]	−10.0 ± 0.1	2074	4.8 ± 0.1	9.6 ± 1.0
TWEAK	Fn14 (1)	70 ± 10[e]	−9.8 ± 0.1	na[o]	na[o]	na[o]
CD40L	CD40 (4)	13000 ± 2000[f]	−6.7 ± 0.1	1830 ± 53	3.7 ± 0.1	9.1 ± 1.1
BAFF	BR3 (1/2)	15 ± 5[g]	−10.7 ± 0.2	1335 ± 12	8.0 ± 0.7	15.5 ± 1.5
	BCMA (1)	1500 ± 200[g]	−8.0 ± 0.1	1278 ± 60	6.2 ± 0.2	14.0 ± 1.6
	TACI (2)	13[h]	−10.8	na[o]	na[o]	na[o]
APRIL	BR3 (1/2)	>3000[g]	>−7.5	na[o]	na[o]	na[o]
	BCMA (1)	15 ± 8[g]	−10.7 ± 5	1524 ± 27	7.0 ± 0.2	13.6 ± 1.3
	TACI (2)	11[h]	−10.9	1675 ± 61	6.5 ± 0.2	12.5 ± 1.2
OX40L	OX40 (3.5)	190[i]	−9.2	2004 ± 1	4.6 ± 0.02	9.6 ± 1.0
TL1A	DcR3 (4)	56[j]	−9.9	2044 ± 96[n]	4.8 ± 0.12	9.7 ± 1.0
FasL		270[j]	−9.0	na[o]	na[o]	na[o]
LIGHT		14[j]	−10.7	na[o]	na[o]	na[o]
	LTβR (4)	38[k]	−10.1	na[o]	na[o]	na[o]
LTα1β2		48[k]	−10.0	na[o]	na[o]	na[o]
TRAIL	OPG (3.5)	21[l]	−10.5	na[o]	na[o]	na[o]
CD27L	CD27 (2.5)	1−10[m]	−10.9 to −12.3	na[o]	na[o]	na[o]

[a]Calculated from $\Delta G_0 = -RT \ln K_D$. [b]Calculated as described in Materials and Methods. PDB entries are as follows: LTα−TNFR1, 1TNR; CD40L−CD40, 3QD6; BAFF−BR3, 1OQE; BAFF−BCMA, 1OQD; APRIL−BCMA, 1XU2; APRIL−TACI, 1XU1; OX40L−OX40, 2HEV; TL1A−DcR3, 3K51 and 3MI8. The TNFα−TNFR1 cocrystal structure was a personal communication from L. Silvian. Except where otherwise noted, uncertainty limits represent the spread of values where two or more geometries were observed in the unit cell. [c]Calculated from $\Delta G_0/\Delta$ASA, as described in the text. [d]Calculated from eq 2, as described in the text. The uncertainty limits are derived primarily from the uncertainty in ΔS_{config} (see the text). [e]From this study. [f]From ref 21. [g]From ref 20. [h]From refs 6, 18, and 19. [i]From ref 79. [j]From ref 14. [k]From ref 80. [l]From ref 81. [m]From ref 82. [n]Uncertainty limits reflect a small difference between two independent structures, PDB entries 3K51 and 3MI8. [o]Not available (i.e., no crystal structure for the complex has been reported).

were measured by surface plasmon resonance spectroscopy using a Biacore3000 instrument. The homotrimeric ligand (i.e., TWEAK, TNFα, or LTα) was immobilized on the surface of a Biacore CM5 sensor chip as described in Materials and Methods, and a soluble monomeric construct of the appropriate receptor extracellular domain was passed over this derivatized sensor surface at various concentrations. Capturing the multivalent binder on the sensor surface and having the monovalent partner in solution ensured that the results reflected single-site receptor binding uninfluenced by avidity effects. We have previously shown for other TNF−TNFR interactions that this experimental configuration results in reliable single-site binding affinities.[20] Figure 2A shows the set of binding curves measured for various concentrations of soluble Fn14, ranging from 40 to 360 nM, binding to TWEAK captured on the sensor chip surface. The black curves show the experimental data, while the overlaid red lines represent a global fit of the entire data set to a single-site binding model. The fit returned a value for the association rate constant k_a of $(1.4 \pm 0.3) \times 10^5$ M^{-1} s^{-1} and a dissociation rate constant k_d of $(9.2 \pm 1.9) \times 10^{-3}$ s^{-1} ($n = 3$). The k_d/k_a ratio gave an equilibrium dissociation constant K_D of 65 ± 1 nM. The inset plot shows the equilibrium binding signal, R_{eq}, as a function of Fn14 concentration, fitted to a hyperbolic, single-site binding equation, giving an alternative means to compute the binding affinity in a manner independent of kinetics. The curve fit returned a K_D value of 76 ± 9 nM ($n = 5$), in excellent agreement with the value calculated from the kinetic analysis. Figure 2B shows comparable data for 1.5−15 nM TNFR1 binding to TNFα immobilized on the sensor chip. Global fitting of the kinetic data returned a value for association rate constant k_a of $(5.8 \pm 1.9) \times 10^5$ M^{-1} s^{-1} and a dissociation rate constant k_d of $(7.5 \pm 2.4) \times 10^{-4}$ s^{-1}, corresponding to an equilibrium binding affinity K_D of 1.4 ± 0.4 nM ($n = 3$). In this experiment, the low concentrations of the receptor required for binding meant that most of the progress curves did not reach equilibrium during the longest achievable protein injection phase, and therefore, a separate analysis of R_{eq} versus TNFR1 concentration was not attempted in this case. For TNFR1 (15−150 nM) binding to immobilized LTα (Figure 2C), global fitting of the kinetic data returned the following: $k_a = (1.7 \pm 0.2) \times 10^5$ M^{-1} s^{-1}, and $k_d = (9.2 \pm 2.8) \times 10^{-3}$ s^{-1}. They correspond to a binding affinity K_D of 46 ± 17 nM ($n = 3$). The global curve fit was not of the same quality for this ligand−receptor combination as for the other two, with the data showing a modest but nonetheless pronounced systematic deviation from the fit, possibly indicating a small amount of slow, nonspecific binding of the receptor to the derivatized sensor surface. However, the plot of R_{eq} versus TNFR1 concentration (Figure 2C, inset) fit well to a hyperbolic binding equation, giving a K_D of 57 ± 7 nM ($n = 4$) that agrees with the results of the kinetic analysis, suggesting that a K_D value of ∼50 nM is a reasonable estimate for the single-site binding affinity for this ligand−receptor pair. Notably, each of the three K_D values we measure here is 10−100-fold higher than literature values for the same three ligand−receptor interactions obtained using bivalent receptor constructs.[37−42] This observation further supports the notion that our K_D values represent single-site binding affinities uncontaminated by avidity effects, as we have shown to be the case for other TNF−TNFR interactions we have characterized using the same method.[20] The K_D values for the three ligand−receptor pairs shown in Figure 2, together with the single-site binding affinities for additional TNF−TNFR complexes from our own previous

dx.doi.org/10.1021/bi301039t | Biochemistry 2012, 51, 9124−9136

work and all other published values we could find, are listed in Table 2.

To determine how much binding energy each TNF−TNFR binding interface generates per unit of contact area, we calculated the amount of solvent-accessible surface area buried per receptor−ligand interface (ΔASA) for each of the complexes in Table 2 for which a high-resolution structure is available. Solvent-accessible surface areas were calculated using a spherical probe with a radius of 1.4 Å, as described in Materials and Methods. The results are listed in Table 2. Figure 3 shows the standard molar free energy of binding, ΔG_0 (=$-RT$ ln K_D), plotted against ΔASA for each of the nine receptor−ligand complexes for which both single-site binding affinities and experimental complex structures are available. To scale the binding efficiencies of the TNF−TNFR complexes from Table 2 relative to the maximal achievable binding efficiency for a reversible protein−protein interaction, we performed the same analysis on the large set of PPI complexes contained in the Cancer Research UK Protein−protein Interaction Affinity (PPIA) Database.[43] This database contains 144 PPI complexes for which both reliable binding affinities and experimental complex structures have been reported. The database also gives ΔASA values for complex formation, calculated using a method equivalent to the one we employed for the TNF−TNFR complexes in this study.[27] A plot of ΔG_0 against ΔASA for these 144 PPI complexes is also shown in Figure 3, overlaid on the values for the nine TNF−TNFR family complexes from this study. The results in Figure 3 and Table 2 show that the BAFF−BR3 complex, the most compact and efficient TNF−TNFR complex in our test set, displays a binding efficiency that falls close to the highest values observed for complexes in the PPIA database. Other TNF−TNFR family complexes showed a range of lower binding efficiencies. Although no crystal structure is available for the TWEAK−Fn14 complex, on the basis of the small size of this receptor and the relatively high single-site binding affinity that we report here (Table 2), it is expected that this pair also will show a very high binding efficiency.

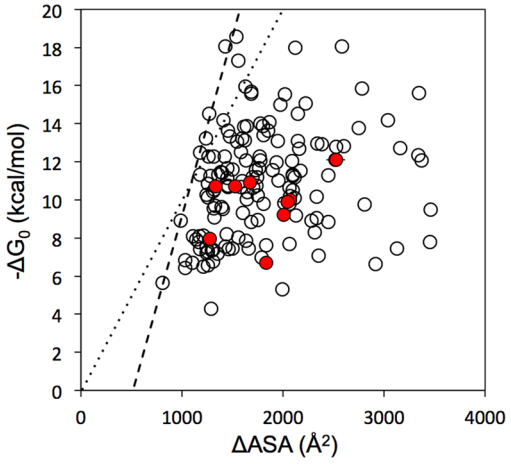

Figure 3. Binding energies for the eight TNF−TNFR family complexes (red ●) and 144 reversible protein−protein complexes from the Cancer Research UK Protein−protein Interaction Database (○), plotted as a function of the surface area buried at the binding interface. The dotted line represents the estimated maximal observed binding efficiency for these complexes, if this quantity is calculated simply as $\Delta G_0/\Delta$ASA. The dashed line represents the preferred interpretation, in which a threshold level of ∼500 Å^2 of interface area is required to form a measurably stable complex, and each additional square angstrom of buried surface area stabilizes the complex by a further ∼20 cal/mol.

As expected,[22,23,27] Figure 3 shows that there is no overall correlation between binding energy and contact area. However, by looking at those complexes that provide the highest binding energy per unit contact area, we can establish a value for the maximal binding efficiency that is observed across this large and diverse set of complexes. One approach to analyzing this data set would be simply to divide ΔG_0 by the interface area for each complex, taking the highest values for $\Delta G_0/\Delta$ASA as the maximal observed binding efficiencies, as illustrated by the dotted line in Figure 3. However, interpreting the data in this way is invalid for the following reason. The K_D values used to calculate ΔG_0 are based on a standard state with a concentration of 1 M. A ΔG_0 value of 0 therefore does not correspond to a complete absence of binding, but rather to a K_D of 1 M (i.e., no change in free energy upon binding under standard state conditions at 1 M). Thus, the choice of a ΔG_0 of 0 as the origin for the dotted line in Figure 3, implying a K_D of 1 M at zero contact interface, is arbitrary and likely incorrect. An alternative approach to estimating the maximal binding efficiency of the protein−protein complexes represented in Figure 3 is based on the observation that the upper left boundary of the data can be roughly defined by the dashed line in Figure 3, which has a slope of ∼20 cal mol^{-1} Å^{-2}. This line represents the interpretation that PPI interfaces that bury less than ∼500 Å^2 of surface area do not support the formation of a stable complex (defined here as a complex with a K_D of ≤1 M), but above this threshold each additional square angstrom of contact surface generates a maximum of ∼20 cal/mol of binding energy. Interestingly, this notion agrees with previous suggestions that stable PPI complexes have a minimal interface size of ∼600 Å^2.[44,45]

DISCUSSION

The binding affinity between a protein and its ligand, whether with another protein or with a small molecule, depends not only on the surface area of contact but also on the number and nature of the interatomic interactions that are formed. When binding is multivalent, binding strength can become further increased through avidity effects.[46] In our study, we are interested in obtaining an empirical estimate for the maximal interaction energy that a reversible and monovalent protein−protein binding interface of a given size can generate using the structural elements and interaction modes available to it. The answer to this question not only improves our fundamental understanding of molecular recognition at protein−protein interfaces, but also has practical applications for the affinity maturation of proteins through protein engineering, and for identifying when a natural protein−protein interface might have evolved to achieve properties beyond simply binding.

The results shown in Figure 3 suggest that a threshold level of contact area, amounting to ∼500 Å^2, is required for the formation of a minimally stable protein−protein complex. The idea of a minimal interface size has been proposed previously by Thornton[44] and Bogan and Thorn,[45] on the basis that their comprehensive surveys of reversible protein−protein complexes for which cocrystal structures were available revealed none with contact areas (ΔASA) of less than ∼600 Å^2, as indeed there are none among the 144 complexes from the PPIA database shown in Figure 3.[43] The existence of a minimal

dx.doi.org/10.1021/bi301039t | Biochemistry 2012, 51, 9124−9136

interface size makes intuitive sense when one considers that, for a reversible complex to exist to any significant degree even at a concentration of 1 M, some interaction energy is required to compensate for the entropic cost of freezing out the independent rigid-body translational and overall rotational motions of the binding partners so they can come together into a complex. Specifically, for the bound and unbound states to have equal free energies at 1 M (i.e., $K_D \sim 1$ M), resulting in a standard molar free energy for binding ΔG_0 of 0 kcal/mol, the interaction between two proteins must generate an amount of binding energy that is equal to $T\Delta S_{config}$, where ΔS_{config} is the configurational entropy cost of colocalizing two molecules from a 1 M solution. Thus, the measured value of ΔG_0 reflects the total binding energy between the interacting proteins, ΔG_{bind}, minus $T\Delta S_{config}$, or expressed in a different way

$$\Delta G_{bind} = \Delta G_0 + T\Delta S_{config} \quad (1)$$

For small molecule systems, ΔS_{config} has been estimated to have a value of ~35 cal mol^{-1} K^{-1},[47] which corresponds to a free energy cost of ~10.5 kcal/mol at 298 K (the temperature of the measurements plotted in Figure 3). Both overall translational entropy and overall rotational entropy are relatively insensitive to molecular size, scaling with the log of the molecular weight,[48] suggesting that the corresponding values for protein molecules might not be very much larger than these small molecule-derived estimates. Moreover, the entropic contribution of new vibrational modes within the complex also scales with molecular size and complexity[47] and will partly compensate for any size-dependent increase in $T\Delta S_{config}$ for larger molecules. Indeed, other estimates for $T\Delta S_{config}$ at 298 K, including estimates for protein−ligand and protein−protein interactions, fall in the range of 6−15 kcal/mol.[49−53] Whatever the exact value of ΔS_{config}, it is clear that ΔG_0 represents only a portion of the overall interaction energy between the two interacting molecules, with the true interaction energy being larger than ΔG_0 by several kilocalories per mole, as expressed in eq 1.

The concept outlined above can be applied to the data from Figure 3 as follows. If each square angstrom of contact area between the two proteins generates up to 20 cal/mol of binding energy, and we take a value for $T\Delta S_{config}$ of ~10 kcal/mol, then the minimal amount of contact area required to "pay for" $T\Delta S_{config}$ and thus allow a minimally stable complex with a K_D of 1 M (i.e., $\Delta G_0 = 0$) will equal 10000/20, which equals 500 Å^2. This value is identical to the threshold of ~500 Å^2 we estimated by extrapolation in Figure 3 and is very close to the minimal PPI interface size of ~600 Å^2 observed by Thornton[44] and Bogan and Thorn.[45] The agreement with these prior reports becomes stronger still if it is considered that 1−10 mM probably better reflects the weakest complexes that can be detected experimentally, which the dashed line in Figure 3 shows to correspond to a minimal interface area of ~600−650 Å^2. Our analysis therefore provides a clear, quantitative rationale for these previous observations of a minimal protein−protein interface size. We propose, therefore, that the most efficient reversible protein−protein interactions generate ~20 cal mol^{-1} Å^{-2} of surface area buried at the interface, but that the first ~10 kcal/mol of binding energy is not expressed in ΔG_0 but instead goes to pay the entropic cost for complex formation from a 1 M standard state. This interpretation corresponds to the dashed line in Figure 3.

An important consequence of this interpretation is that calculating the binding efficiency simply by dividing ΔG_0 by ΔASA underestimates the true or intrinsic binding efficiency for these interactions, which is more accurately given by the equation

$$BE_{intr} = (\Delta G_0 + T\Delta S_{config})/\Delta ASA \quad (2)$$

where $T\Delta S_{config}$ can conveniently be considered to have a value of approximately 10 kcal/mol at 298 K. Henceforth, we will distinguish binding efficiencies calculated with and without the correction for $T\Delta S_{config}$ by calling the value of the simple ratio $\Delta G_0/\Delta ASA$ an "apparent" binding efficiency, while a value calculated from eq 2 will be termed an "intrinsic" binding efficiency, by analogy with the well-established distinction between expressed and intrinsic binding energy.[54] Intrinsic binding efficiencies reflect the full interaction energy that the proteins generate per square angstrom of surface area buried at the binding interface, whereas the apparent binding efficiency underestimates the interaction energy density to a degree that depends on the magnitude of ΔG_0.

A maximal intrinsic binding efficiency of ~20 cal mol^{-1} Å^{-2} is consistent with a variety of previous estimates for the amount of energy generated by burial of different atom types at protein interfaces or protein interiors. For example, Zhou and Zhou[55] report a range of 12−28 cal mol^{-1} Å^{-2} for the free energy change accompanying the transfer of different amino acids from an aqueous solution to become buried within a protein interior or at a protein−protein interface.[55] Similarly, several groups have estimated that the energy arising from the hydrophobic effect for the burial of apolar amino acids at a PPI interface generates ~20−30 cal mol^{-1} Å^{-2},[23,56−58] though both lower and higher values have been proposed.[25,59,60] It has been proposed that the hydrophobic effect is generally the dominant force in protein−protein binding.[24,26,61] We show here that this level of binding energy is indeed characteristic of what is seen experimentally for the most efficient reversible protein−protein interactions.

Importantly, the set of PPI complexes that comprises the PPIA database includes the strongest reversible protein−protein interactions for which affinities and cocrystal structures have been reported to date. These include colicin E9 nuclease−Im9 (K_D = 24 fM),[62,63] ribonuclease A−ribonuclease inhibitor (K_D = 59 fM),[64] trypsinogen−BPTI (K_D = 60 fM),[65] and barnase−barstar (K_D = 200 fM),[66] as well as many other picomolar or subnanomolar complexes.[43] All of these very high affinity complexes are included in Figure 3, and all of them fall within the limit defined by the dashed line in that figure. Indeed, in searching the literature, we were unable to identify any reversible PPI complex that exceeds the upper limit to the single-site binding efficiency defined by the dashed line in Figure 3.

Intrinsic binding efficiencies for the nine TNF−TNFR family complexes considered in this study, calculated using eq 2, are listed in Table 2. The values range from a high of ~16 cal mol^{-1} Å^{-2} for the BAFF−BR3 complex, corresponding to ~80% of the proposed maximal achievable value of 20 cal mol^{-1} Å^{-2}, to a low of approximately half of this amount for larger TNFα−TNFR1, LTα−TNFR1, CD40L−CD40, and OX40L−OX40 complexes. It is noteworthy that, considered in terms of binding efficiency, the different TNF−TNFR complexes appear to be grouped by the number of CRDs present in their receptor extracellular domain. Thus, all of the receptors containing 3.5 or 4 CRDs generate from 8.8 to 9.7 cal mol^{-1} Å^{-2} of binding energy, while the receptors containing no more than 1 CRD generate 13.6−15.5 cal mol^{-1} Å^{-2} of binding energy. TACI, the

only one among these nine receptors that contains more than 1 but fewer than 3.5 CRDs, shows an intermediate binding efficiency of 12.5 cal mol^{-1} Å^{-2} in its interaction with APRIL, though Figure 3 suggests it might best be considered to cluster with the small receptors.

It initially seems counterintuitive that the BAFF–BCMA complex (K_D ~ 1500 nM) would appear in the high-binding efficiency group with the BAFF–BR3 complex (K_D ~ 15 nM), despite its 100-fold lower binding affinity. Similarly, the complex of the 4-CRD receptor CD40 with CD40L (K_D ~ 13000 nM) actually generates more binding energy per square angstrom than does the much higher affinity complex of TNFα with TNFR1 (K_D ~ 1.4 nM; also 4 CRDs); both of these complexes fall into the low-binding efficiency group. These seeming anomalies highlight the fact that, because of the large $T\Delta S_{config}$ term in eq 2, the intrinsic binding efficiency is more sensitive to differences in ΔASA than it is to differences in ΔG_0. Because ΔG_0 represents only a portion of the observed interaction energy between the proteins, substantial differences in ΔG_0 corresponding to differences of several orders of magnitude in binding affinity represent relatively modest variations in the overall interaction energy. Thus, the difference in binding efficiency between the large and small TNFRs manifested in Table 2 arises from a significant generic difference in the overall interface area for large versus small receptors and is not greatly affected by differences of a few kilocalories per mole in ΔG_0 within each receptor class.

To further explore the relationship between the number of CRDs in a given receptor and the amount of surface buried at the binding interface, we calculated ΔASA for each separate CRD of each receptor. Figure 4 and Table S1 of the Supporting Information show that, for each of these complexes except the OX40–OX40L complex, the buried surface area is dominated by interaction of one CRD, regardless of how many CRDs the receptor contains. For receptors with more than one CRD, this dominant domain is invariably CRD2 (where the CRDs are numbered, according to convention, starting from the N-terminal end of the receptor sequence). Moreover, among these eight complexes, the dominant domain buries a relatively constant 1600 ± 300 Å^2 of solvent-accessible surface area (ligand and receptor) at the interface, corresponding to between 75 and 100% of the total ΔASA for the entire complex. The OX40–OX40L complex is an exception to this trend, in that CRD1 contributes almost as much to the total contact area as does CRD2. BR3 is also something of a special case; it contains only a fragment of a CRD, but as one can see in Figure 1C and Figure S2 of the Supporting Information, this receptor contains some additional structure that interacts with its ligand adjacent to but somewhat outside the canonical receptor binding groove, toward the "south pole" of the BAFF trimer. Thus, although Figure 4 indicates BR3 buries ~1300 Å^2 of surface area at each ligand–receptor interface, not very different from the amount buried by the single-CRD receptor BCMA, BR3 achieves this extent of contact partly through additional interactions mediated by residues outside its fragmentary CRD. It is noteworthy that, for TNFR1, DcR3, and CD40L, even when all the binding energy is attributed to contact with the dominant CRD alone, those dominant CRDs would still display somewhat a lower binding efficiency than those found for the small receptors. Therefore, the lower binding efficiencies seen for the large receptors do not simply reflect the efficient binding of a single dominant CRD "diluted" by much less efficient contacts through one or more additional

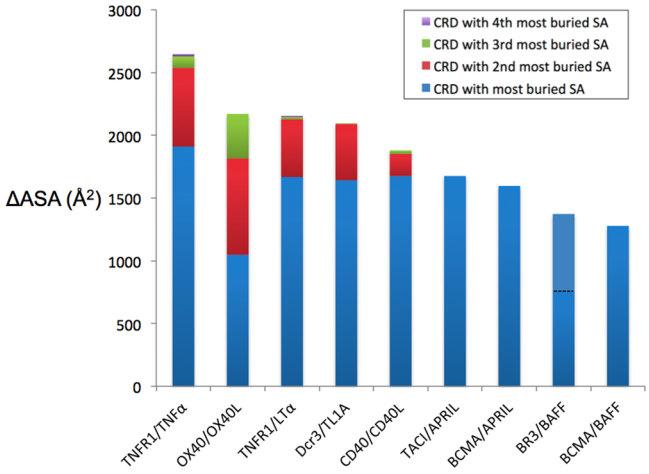

Figure 4. Stacked histogram showing the solvent-accessible surface area buried in each of the TNF–TNFR family complexes examined in this study, broken down to reveal the contribution of each CRD. Data are stacked in order of the amount of surface area buried, as indicated by the key. The bar representing the data for the BR3–BAFF complex is divided into a lower portion indicating the contribution of the fragmentary CRD present in BR3, and an upper portion showing the contribution of the unique non-CRD portion of the receptor (see the text and Figure S2 of the Supporting Information). Numerical values for the ΔASA buried by each CRD of each receptor are listed in Table S1 of the Supporting Information. Note that structures are available for four other TNF–TNFR family complexes, not included in this study because no reliable single-site receptor binding affinities have been reported. These complexes conform to the pattern shown in the figure, in that they contain one receptor CRD that buries >1000 Å^2 of surface area, though in two cases, the osteoprotegerin–RANKL (PDB entry 3URF) and DR5–TRAIL (PDB entries 1D4V and 1DU3) complexes, domain 3 also buries substantial surface area, similar to the OX40–OX40L complex in the figure.

CRDs. Instead, the binding efficiency of the dominant CRD is demonstrably lower for the large receptors than for BR3, BCMA, and TACI. Interestingly, the dominant domain in the large receptors (i.e., those with 3.5 or 4 CRDs) interacts at a different location within the receptor binding groove on the ligand compared to the small receptors BR3, BCMA, and TACI. Specifically, CRD2 of the larger receptors TNFR1, CD40, DcR3, and OX40 binds in the equatorial region of the ligand, while the single-CRD receptors and TACI instead bind close to the "southern" end of the ligand farthest from the N- and C-termini (see Figure S2 of the Supporting Information). Whether there are generic structural or physicochemical differences between the equatorial and southern sites on TNF family ligands that contribute to the distinct binding efficiencies observed for the TNFR domains that bind at these different locations is unclear.

These results highlight the fact that the evolution of these ligand–receptor pairs does not appear to place any premium on minimizing the interface area or the number of CRDs required in the receptor for strong and specific binding. TNF–TNFR proteins are found in primitive multicellular organisms, including invertebrates such as cnidaria, mollusks, and arthropods.[67] For example, *Drosophila* has a single TNF family ligand, eiger, and a single TNFR family receptor, wengen. The extracellular domain of wengen comprises only a single CRD, which most closely resembles the mammalian CRD structure designated A1C2.[68] Interestingly, the small TNFR family receptors in humans, namely, BR3, BCMA, Fn14, and TACI,

dx.doi.org/10.1021/bi301039t | *Biochemistry* 2012, 51, 9124–9136

also possess an A1C2 or the closely related A1D2 structure,[69] which otherwise is found only in the fourth domain of TNFR1 and not in any of the two dozen other human TNFR family receptors, all of which have multiple CRDs.[15,70] The majority of TNF−TNFR pairs for which single-site binding data are available show interaction affinities of 10−100 nM (Table 2). Our results suggest that the footprint made by a single CRD binding to a TNF family ligand, minimally comprising ∼1300 Å^2, represents more or less the smallest contact region that can achieve a reversible protein−protein interface with this affinity. Notably, even these relatively small interfaces can achieve not only good affinity but also high selectivity. For example, BAFF is 100-fold selective for BR3 versus BCMA, whereas the homologous ligand APRIL shows an even greater opposite selectivity for these two receptors.[20] Moreover, TACI, which has two CRDs but uses only one of them for binding, interacts with these same binding sites on BAFF and APRIL with essentially identical affinities of ∼10 nM.[19] We can therefore conclude that the evolution of receptors with additional CRDs and larger ligand−receptor contact interfaces was not driven by a need for increased affinity or selectivity. The evolutionary pressure behind the development of these larger TNFR family receptors is presently unclear but perhaps in some cases might be related to additional functional interactions beyond ligand binding, such as the receptor−receptor interactions mediated by the N-terminal PLAD domains present in some family members.[71]

It can be argued that by restricting our analysis to reversible protein−protein complexes, while omitting constitutive protein oligomers that might be expected to have higher binding affinities, we might have biased our analysis to exclude the most efficient PPI complexes. However, as has been noted previously,[44,72−74] constitutive and transient protein−protein interactions represent quite different phenomena. This is because proteins that engage in transient PPI complexes must necessarily possess a structure that allows each binding partner to exist as a stable, soluble monomer in the unbound state, which imposes significant constraints on the amount of hydrophobic surface area and other physicochemical properties of the binding site. Constitutive PPI complexes evolved under no such constraint. It is therefore likely that constitutive PPI interactions have a different and possibly higher upper limit for the achievable binding efficiency than we see here for transient, reversible complexes, because constitutive complexes use interaction modes that are not available to the more physicochemically balanced surfaces that necessarily constitute transient PPI binding sites. By restricting our analysis to reversible PPI complexes, we have established the maximal binding efficiency associated with PPI binding sites on stable, soluble proteins.

The estimate for the maximal achievable binding efficiency for a reversible, monovalent protein−protein interaction mentioned above potentially provides useful guidance for protein engineering efforts in increasing the binding affinity for another protein or introducing a binding site for a new protein binding partner. Specifically, it provides an explicit estimate for the minimal size that a monovalent contact interface must possess to achieve the desired level of binding affinity. From the equation for the dashed line in Figure 3, we can say that for a maximally efficient PPI interface the interface area is related to binding affinity by the inequality $\Delta ASA > 500 - 0.05RT \ln K_D$, where ΔASA is the amount of solvent-accessible surface area buried at the interface, in square angstroms, and R is the molar gas constant expressed in units of calories per kelvin per mole. At a temperature of 298 K, this expression simplifies to

$$\Delta ASA > 500 - 30 \ln K_D \quad (3)$$

Thus, for example, if the goal is to engineer an existing contact interface to increase its binding affinity to a value of 1 nM, our results suggest that such an effort is likely to succeed only for a monovalent interaction if the contact interface has a ΔASA of >1100 Å^2. Achieving this affinity through modification of a significantly smaller interface would require that the resulting complex exceed the maximal binding efficiency seen in our study. Such an outcome may not be impossible, but at the very least, it would presumably require an interaction mechanism that differs from those employed by the large set of proteins included in our study, and in particular it would likely be difficult to achieve such strong binding while maintaining the ability of the engineered protein to exist as a stable, soluble monomer in its unbound form. Our analysis also potentially provides an objective basis for assessing the progress of protein engineering efforts aimed at enhancing binding affinity for protein targets, for example, in the affinity maturation of monovalent binders such as single-domain antibodies and other monovalent antibody constructs,[75] fibronectin-based affinity scaffolds,[76] engineered ankyrin repeats,[77] and stapled peptides.[78] Equation 3 represents a quantitative expectation against which the efficiency of any engineered interface for which a crystal structure is available can be assessed. Complexes with affinities below that given by eq 3 potentially have room for further improvement, whereas once the proposed limit for binding energy per area has been reached, our analysis implies that further improvement will likely be very difficult. On the other hand, our analysis highlights the fact that relatively modest increases in contact area can result in large increases in binding affinity, if the newly contacted atoms interact with high binding efficiency. For example, enhancing the affinity of a complex by 10-fold, corresponding to ∼1.4 kcal/mol of binding energy, requires as little as 1400/20 = 70 Å^2 of additional contact area, provided that this new area contributes the maximal achievable binding efficiency of 20 cal mol^{-1} Å^{-2}. This is a very small increase in interface area, corresponding to the burial of just two or three additional non-hydrogen atoms on each partner. Thus, just as adding a small substituent to a small molecule ligand can result in a substantial increase in binding affinity, increasing the extent of a protein−protein binding interface by a few atoms can do the same for a PPI complex. In cases where eq 3 suggests that the interface being engineered is at the limit of the affinity achievable for its size, substantial further enhancement of binding might be achieved by making amino acid substitutions at the periphery of the interface to bury just a few tens of additional square angstroms of protein surface.

Overall, our analysis suggests that binding efficiency represents a useful concept for the quantitative understanding of reversible protein−protein binding, and that its application can be used to derive benchmarks with potential value for protein drug design and protein engineering.

■ ASSOCIATED CONTENT

Supporting Information

Surface areaa buried by each CRD of the each TNF family receptor, for the nine TNF−TNFR family complexes discussed here (Table S1), the results of SDS−PAGE characterization of TNFR1 and Fn14 (Figure S1), and structures of the TNF−

TNFR family complexes, with the individual CRDs that contribute the most area to the receptor−ligand binding interface highlighted (Figure S2). This material is available free of charge via the Internet at http://pubs.acs.org.

AUTHOR INFORMATION

Corresponding Author

*Department of Chemistry, Boston University, 590 Commonwealth Ave., Boston, MA 02215. Telephone: (617) 353-2488. E-mail: whitty@bu.edu.

Funding

This work was supported, in part, by Grants GM094551 and GM087469 to A.W. from the National Institutes of Health.

Notes

The authors declare the following competing financial interest(s): At the time this research was performed, E.S.D. was an employee and shareholder of Biogen Idec, a company that has a commercial interest in research on TNF−TNF receptor family members. A.W. is also a shareholder of Biogen Idec.

ACKNOWLEDGMENTS

We thank Laura Silvian for permission to use her unpublished cocrystal structure of the TNFα−TNFR1 complex for the surface area calculations for this complex in Table 2, Figure 4, and Table S1 of the Supporting Information, Jessica Friedman for performing the HTRF binding affinity comparison of the soluble TNFR1 against TNFR1 preparations from other sources, Mia Rushe for her generous assistance in addressing the reviewers' comments, and Elizabeth Villar and Dmitri Beglov for their assistance with the protein surface area calculations. We also thank Karen Allen, Sandor Vajda, and Peter Tonge for helpful discussions.

ABBREVIATIONS

ΔASA, amount of solvent-accessible surface area buried at an interface; APRIL, a proliferation-inducing ligand, also known as TNFSF13; BAFF, B cell-activating factor belonging to the TNF family, also known as BLyS, TALL-1, and TNFSF13B; BAFFR, BAFF receptor, also known as BR3 or TNFRSF13C; BCMA, B cell maturation antigen, also known as TNFRSF17; BR3, BAFF receptor, also known as BAFFR or TNFRSF13C; CD40, cluster of differentiation 40, also known as TNFRSF5; CD40L, CD40 ligand, also known as CD154 or TNFSF5; CRD, cysteine rich domain; DcR3, decoy receptor 3, also known as TNFRSF6B; Fn14, fibronectin growth factor-inducible 14, also known as TWEAKR, CD266, or TNFRSF12A; LTα, lymphotoxin-α, also known as TNFβ or TNFSF1; OX40, MRC OX40 mAb antigen, also known as CD134 or TNFSF4; OX40L, OX40 ligand, also known as gp34, CD252, or TNFSF4; PDB, Protein Data Bank; PPI, protein−protein interaction; PPIA Database, Protein−protein Interaction Affinity Database; TACI, transmembrane activator and CAML interactor, also known as CD267 or TNFRSF13B; TL1A, TNF ligand-related 1A, also known as TNFSF15; TNF, tumor necrosis factor; TNFR, tumor necrosis factor receptor; TWEAK, TNF-related weak ligand, also known as APO3L or TNFSF12.

REFERENCES

(1) Kuntz, I. D., Chen, K., Sharp, K. A., and Kollman, P. A. (1999) The maximal affinity of ligands. *Proc. Natl. Acad. Sci. U.S.A. 96*, 9997−10002.

(2) Hopkins, A. L., Groom, C. R., and Alex, A. (2004) Ligand efficiency: A useful metric for lead selection. *Drug Discovery Today 9*, 430−431.

(3) Lipinski, C. A., Lombardo, F., Dominy, B. W., and Feeney, P. J. (2001) Experimental and computational approaches to estimate solubility and permeability in drug discovery and development settings. *Adv. Drug Delivery Rev. 46*, 3−26.

(4) Naismith, J. H., and Sprang, S. R. (1998) Modularity in the TNF-receptor family. *Trends Biochem. Sci. 23*, 74−79.

(5) Banner, D. W., D'Arcy, A., Janes, W., Gentz, R., Schoenfeld, H. J., Broger, C., Loetscher, H., and Lesslauer, W. (1993) Crystal structure of the soluble human 55 kd TNF receptor-human TNF β complex: Implications for TNF receptor activation. *Cell 73*, 431−445.

(6) An, H. J., Kim, Y. J., Song, D. H., Park, B. S., Kim, H. M., Lee, J. D., Paik, S. G., Lee, J. O., and Lee, H. (2011) Crystallographic and mutational analysis of the CD40-CD154 complex and its implications for receptor activation. *J. Biol. Chem. 286*, 11226−11235.

(7) Hymowitz, S. G., Christinger, H. W., Fuh, G., Ultsch, M., O'Connell, M., Kelley, R. F., Ashkenazi, A., and de Vos, A. M. (1999) Triggering cell death: The crystal structure of Apo2L/TRAIL in a complex with death receptor 5. *Mol. Cell 4*, 563−571.

(8) Liu, C., Walter, T. S., Huang, P., Zhang, S., Zhu, X., Wu, Y., Wedderburn, L. R., Tang, P., Owens, R. J., Stuart, D. I., Ren, J., and Gao, B. (2010) Structural and functional insights of RANKL-RANK interaction and signaling. *J. Immunol. 184*, 6910−6919.

(9) Luan, X., Lu, Q., Jiang, Y., Zhang, S., Wang, Q., Yuan, H., Zhao, W., Wang, J., and Wang, X. (2012) Crystal Structure of Human RANKL Complexed with Its Decoy Receptor Osteoprotegerin. *J. Immunol. 189*, 245−252.

(10) Mongkolsapaya, J., Grimes, J. M., Chen, N., Xu, X. N., Stuart, D. I., Jones, E. Y., and Screaton, G. R. (1999) Structure of the TRAIL-DR5 complex reveals mechanisms conferring specificity in apoptotic initiation. *Nat. Struct. Biol. 6*, 1048−1053.

(11) Mukai, Y., Nakamura, T., Yoshikawa, M., Yoshioka, Y., Tsunoda, S., Nakagawa, S., Yamagata, Y., and Tsutsumi, Y. (2010) Solution of the structure of the TNF-TNFR2 complex. *Sci. Signaling 3*, ra83.

(12) Ta, H. M., Nguyen, G. T., Jin, H. M., Choi, J., Park, H., Kim, N., Hwang, H. Y., and Kim, K. K. (2010) Structure-based development of a receptor activator of nuclear factor-kappaB ligand (RANKL) inhibitor peptide and molecular basis for osteopetrosis. *Proc. Natl. Acad. Sci. U.S.A. 107*, 20281−20286.

(13) Compaan, D. M., and Hymowitz, S. G. (2006) The crystal structure of the costimulatory OX40-OX40L complex. *Structure 14*, 1321−1330.

(14) Zhan, C., Patskovsky, Y., Yan, Q., Li, Z., Ramagopal, U., Cheng, H., Brenowitz, M., Hui, X., Nathenson, S. G., and Almo, S. C. (2011) Decoy strategies: The structure of TL1A:DcR3 complex. *Structure 19*, 162−171.

(15) Bodmer, J.-L., Schneider, P., and Tschopp, J. (2002) The molecular architecture of the TNF superfamily. *Trends Biochem. Sci. 27*, 19−26.

(16) Thompson, J. S., Bixler, S. A., Qian, F., Vora, K., Scott, M. L., Cachero, T. G., Hession, C., Schneider, P., Sizing, I. D., Mullen, C., Strauch, K., Zafari, M., Benjamin, C. D., Tschopp, J., Browning, J. L., and Ambrose, C. (2001) BAFF-R, a newly identified TNF receptor that specifically interacts with BAFF. *Science 293*, 2108−2111.

(17) Liu, Y., Hong, X., Kappler, J., Jiang, L., Zhang, R., Xu, L., Pan, C. H., Martin, W. E., Murphy, R. C., Shu, H. B., Dai, S., and Zhang, G. (2003) Ligand-receptor binding revealed by the TNF family member TALL-1. *Nature 423*, 49−56.

(18) Gordon, N. C., Pan, B., Hymowitz, S. G., Yin, J., Kelley, R. F., Cochran, A. G., Yan, M., Dixit, V. M., Fairbrother, W. J., and Starovasnik, M. A. (2003) BAFF/BLyS receptor 3 comprises a minimal TNF receptor-like module that encodes a highly focused ligand-binding site. *Biochemistry 42*, 5977−5983.

(19) Hymowitz, S. G., Patel, D. R., Wallweber, H. J., Runyon, S., Yan, M., Yin, J., Shriver, S. K., Gordon, N. C., Pan, B., Skelton, N. J., Kelley, R. F., and Starovasnik, M. A. (2005) Structures of APRIL-receptor complexes: Like BCMA, TACI employs only a single cysteine-rich domain for high affinity ligand binding. *J. Biol. Chem. 280*, 7218−7227.
(20) Day, E. S., Cachero, T. G., Qian, F., Sun, Y., Wen, D., Pelletier, M., Hsu, Y.-M., and Whitty, A. (2005) Selectivity of BAFF/BLyS and APRIL for Binding to the TNF Family Receptors BAFFR/BR3 and BCMA. *Biochemistry 44*, 1919−1931.
(21) Silvian, L. F., Friedman, J. E., Strauch, K., Cachero, T. G., Day, E. S., Qian, F., Cunningham, B., Fung, A., Sun, L., Shipps, G. W., Su, L., Zheng, Z., Kumaravel, G., and Whitty, A. (2011) Small molecule inhibition of the TNF family cytokine CD40 ligand through a subunit fracture mechanism. *ACS Chem. Biol. 6*, 636−647.
(22) Brooijmans, N., Sharp, K. A., and Kuntz, I. D. (2002) Stability of macromolecular complexes. *Proteins 48*, 645−653.
(23) Horton, N., and Lewis, M. (1992) Calculation of the free energy of association for protein complexes. *Protein Sci. 1*, 169−181.
(24) Olsson, T. S., Williams, M. A., Pitt, W. R., and Ladbury, J. E. (2008) The thermodynamics of protein-ligand interaction and solvation: Insights for ligand design. *J. Mol. Biol. 384*, 1002−1017.
(25) Vallone, B., Miele, A. E., Vecchini, P., Chiancone, E., and Brunori, M. (1998) Free energy of burying hydrophobic residues in the interface between protein subunits. *Proc. Natl. Acad. Sci. U.S.A. 95*, 6103−6107.
(26) Chothia, C. (1974) Hydrophobic Bonding and Accessible Surface-Area in Proteins. *Nature 248*, 338−339.
(27) Kastritis, P. L., Moal, I. H., Hwang, H., Weng, Z. P., Bates, P. A., Bonvin, A. M. J. J., and Janin, J. (2011) A structure-based benchmark for protein-protein binding affinity. *Protein Sci. 20*, 482−491.
(28) Bougouffa, S., and Warwicker, J. (2008) Volume-based solvation models out-perform area-based models in combined studies of wild-type and mutated protein-protein interfaces. *BMC Bioinf. 9*, 448.
(29) Janin, J. (1995) Principles of protein-protein recognition from structure to thermodynamics. *Biochimie 77*, 497−505.
(30) Jakubowski, A., Browning, B., Lukashev, M., Sizing, I., Thompson, J. S., Benjamin, C. D., Hsu, Y. M., Ambrose, C., Zheng, T. S., and Burkly, L. C. (2002) Dual role for TWEAK in angiogenic regulation. *J. Cell Sci. 115*, 267−274.
(31) Browning, J. L., Miatkowski, K., Sizing, I., Griffiths, D., Zafari, M., Benjamin, C. D., Meier, W., and Mackay, F. (1996) Signaling through the lymphotoxin β receptor induces the death of some adenocarcinoma tumor lines. *J. Exp. Med. 183*, 867−878.
(32) He, M. M., Smith, A. S., Oslob, J. D., Flanagan, W. M., Braisted, A. C., Whitty, A., Cancilla, M. T., Wang, J., Lugovskoy, A. A., Yoburn, J. C., Fung, A. D., Farrington, G., Eldredge, J. K., Day, E. S., Cruz, L. A., Cachero, T. G., Miller, S. K., Friedman, J. E., Choong, I. C., and Cunningham, B. C. (2005) Small-molecule inhibition of TNF-α. *Science 310*, 1022−1025.
(33) Foley, S. F., Sun, Y., Zheng, T. S., and Wen, D. (2008) Picomole-level mapping of protein disulfides by mass spectrometry following partial reduction and alkylation. *Anal. Biochem. 377*, 95−104.
(34) Lee, B., and Richards, F. M. (1971) The interpretation of protein structures: Estimation of static accessibility. *J. Mol. Biol. 55*, 379−400.
(35) Hubbard, S., and Thornton, J. (1993) *NACCESS*, Department of Biochemistry and Molecular Biology, University College, London.
(36) UniProt_Consortium (2011) Ongoing and future developments at the Universal Protein Resource. *Nucleic Acids Res. 39*, D214−D219.
(37) Ashkenazi, A., Marsters, S. A., Capon, D. J., Chamow, S. M., Figari, I. S., Pennica, D., Goeddel, D. V., Palladino, M. A., and Smith, D. H. (1991) Protection against endotoxic shock by a tumor necrosis factor receptor immunoadhesin. *Proc. Natl. Acad. Sci. U.S.A. 88*, 10535−10539.
(38) Scallon, B. J., Trinh, H., Nedelman, M., Brennan, F. M., Feldmann, M., and Ghrayeb, J. (1995) Functional comparisons of different tumour necrosis factor receptor/IgG fusion proteins. *Cytokine 7*, 759−770.
(39) Corcoran, A. E., Scallon, B. J., Trinh, H., Chernajovsky, Y., Ghrayeb, J., and Feldmann, M. (1998) Minimal tumor necrosis factor receptor binding protein: Optimum biological activity of a truncated p55 soluble tumor necrosis factor receptor-IgG fusion protein. *Eur. Cytokine Network 9*, 255−262.
(40) Loetscher, H., Gentz, R., Zulauf, M., Lustig, A., Tabuchi, H., Schlaeger, E. J., Brockhaus, M., Gallati, H., Manneberg, M., and Lesslauer, W. (1991) Recombinant 55-kDa tumor necrosis factor (TNF) receptor. Stoichiometry of binding to TNFα and TNFβ and inhibition of TNF activity. *J. Biol. Chem. 266*, 18324−18329.
(41) Donohue, P. J., Richards, C. M., Brown, S. A., Hanscom, H. N., Buschman, J., Thangada, S., Hla, T., Williams, M. S., and Winkles, J. A. (2003) TWEAK is an endothelial cell growth and chemotactic factor that also potentiates FGF-2 and VEGF-A mitogenic activity. *Arterioscler., Thromb., Vasc. Biol. 23*, 594−600.
(42) Brown, S. A., Hanscom, H. N., Vu, H., Brew, S. A., and Winkles, J. A. (2006) TWEAK binding to the Fn14 cysteine-rich domain depends on charged residues located in both the A1 and D2 modules. *Biochem. J. 397*, 297−304.
(43) Protein-Protein Interaction Affinity Database (2010) Cancer Research UK, http://bmm.cancerresearchuk.org.
(44) Jones, S., and Thornton, J. M. (1996) Principles of protein-protein interactions. *Proc. Natl. Acad. Sci. U.S.A. 93*, 13−20.
(45) Bogan, A. A., and Thorn, K. S. (1998) Anatomy of hot spots in protein interfaces. *J. Mol. Biol. 280*, 1−9.
(46) Whitty, A. (2008) Cooperativity and biological complexity. *Nat. Chem. Biol. 4*, 435−439.
(47) Page, M. I., and Jencks, W. P. (1971) Entropic contributions to rate accelerations in enzymic and intramolecular reactions and the chelate effect. *Proc. Natl. Acad. Sci. U.S.A. 68*, 1678−1683.
(48) Page, M. I. (1973) The Energetics of Neighbouring Group Participation. *Chem. Soc. Rev. 2*, 295−323.
(49) Chang, C. E. A., McLaughlin, W. A., Baron, R., Wang, W., and McCammon, J. A. (2008) Entropic contributions and the influence of the hydrophobic environment in promiscuous protein-protein association. *Proc. Natl. Acad. Sci. U.S.A. 105*, 7456−7461.
(50) Lundquist, J. J., and Toone, E. J. (2002) The cluster glycoside effect. *Chem. Rev. 102*, 555−578.
(51) Lazaridis, T., Masunov, A., and Gandolfo, F. (2002) Contributions to the binding free energy of ligands to avidin and streptavidin. *Proteins: Struct., Funct., Genet. 47*, 194−208.
(52) Finkelstein, A. V., and Janin, J. (1989) The price of lost freedom: Entropy of bimolecular complex formation. *Protein Eng. 3*, 1−3.
(53) Luo, R., and Gilson, M. K. (2000) Synthetic Adenine Receptors: Direct Calculation of Binding Affinity and Entropy. *J. Am. Chem. Soc. 122*, 2934−2937.
(54) Jencks, W. P. (1981) On the attribution and additivity of binding energies. *Proc. Natl. Acad. Sci. U.S.A. 78*, 4046−4050.
(55) Zhou, H., and Zhou, Y. (2002) Stability scale and atomic solvation parameters extracted from 1023 mutation experiments. *Proteins 49*, 483−492.
(56) Vajda, S., Weng, Z. P., and DeLisi, C. (1995) Extracting hydrophobicity parameters from solute partition and protein mutation unfolding experiments. *Protein Eng. 8*, 1081−1092.
(57) Karplus, P. A. (1997) Hydrophobicity regained. *Protein Sci. 6*, 1302−1307.
(58) Chan, H. S., and Dill, K. A. (1997) Solvation: How to obtain microscopic energies from partitioning and solvation experiments. *Annu. Rev. Biophys. Biomol. Struct. 26*, 425−459.
(59) Sharp, K. A., Nicholls, A., Fine, R. F., and Honig, B. (1991) Reconciling the Magnitude of the Microscopic and Macroscopic Hydrophobic Effects. *Science 252*, 106−109.
(60) Eisenberg, D., and McLachlan, A. D. (1986) Solvation energy in protein folding and binding. *Nature 319*, 199−203.
(61) Tsai, C. J., and Nussinov, R. (1997) Hydrophobic folding units at protein-protein interfaces: Implications to protein folding and to protein-protein association. *Protein Sci. 6*, 1426−1437.

(62) Wallis, R., Leung, K. Y., Pommer, A. J., Videler, H., Moore, G. R., James, R., and Kleanthous, C. (1995) Protein-protein interactions in colicin E9 DNase-immunity protein complexes. 2. Cognate and noncognate interactions that span the millimolar to femtomolar affinity range. *Biochemistry 34*, 13751−13759.
(63) Keeble, A. H., Joachimiak, L. A., Mate, M. J., Meenan, N., Kirkpatrick, N., Baker, D., and Kleanthous, C. (2008) Experimental and computational analyses of the energetic basis for dual recognition of immunity proteins by colicin endonucleases. *J. Mol. Biol. 379*, 745−759.
(64) Vicentini, A. M., Kieffer, B., Matthies, R., Meyhack, B., Hemmings, B. A., Stone, S. R., and Hofsteenge, J. (1990) Protein chemical and kinetic characterization of recombinant porcine ribonuclease inhibitor expressed in *Saccharomyces cerevisiae*. *Biochemistry 29*, 8827−8834.
(65) Vincent, J. P., and Lazdunski, M. (1972) Trypsin-pancreatic trypsin inhibitor association. Dynamics of the interaction and role of disulfide bridges. *Biochemistry 11*, 2967−2977.
(66) Hartley, R. W. (1993) Directed mutagenesis and barnase-barstar recognition. *Biochemistry 32*, 5978−5984.
(67) Wiens, G. D., and Glenney, G. W. (2011) Origin and evolution of TNF and TNF receptor superfamilies. *Dev. Comp. Immunol. 35*, 1324−1335.
(68) Kauppila, S., Maaty, W. S., Chen, P., Tomar, R. S., Eby, M. T., Chapo, J., Chew, S., Rathore, N., Zachariah, S., Sinha, S. K., Abrams, J. M., and Chaudhary, P. M. (2003) Eiger and its receptor, Wengen, comprise a TNF-like system in *Drosophila*. *Oncogene 22*, 4860−4867.
(69) He, F., Dang, W. R., Saito, K., Watanabe, S., Kobayashi, N., Guntert, P., Kigawa, T., Tanaka, A., Muto, Y., and Yokoyama, S. (2009) Solution structure of the cysteine-rich domain in Fn14, a member of the tumor necrosis factor receptor superfamily. *Protein Sci. 18*, 650−656.
(70) He, B., Chadburn, A., Jou, E., Schattner, E. J., Knowles, D. M., and Cerutti, A. (2004) Lymphoma B cells evade apoptosis through the TNF family members BAFF/BLyS and APRIL. *J. Immunol. 172*, 3268−3279.
(71) Chan, F. K. M., Chun, H. J., Zheng, L. X., Siegel, R. M., Bui, K. L., and Lenardo, M. J. (2000) A domain in TNF receptors that mediates ligand-independent receptor assembly and signaling. *Science 288*, 2351−2354.
(72) Lo Conte, L., Chothia, C., and Janin, J. (1999) The atomic structure of protein-protein recognition sites. *J. Mol. Biol. 285*, 2177−2198.
(73) Ansari, S., and Helms, V. (2005) Statistical analysis of predominantly transient protein-protein interfaces. *Proteins 61*, 344−355.
(74) Whitty, A. (2009) Small-Molecule Inhibitors of Protein-Protein Interactions: Challenges and Prospects. In *Gene family targeted molecular design* (Lackey, K., Ed.) John Wiley & Sons, Hoboken, NJ.
(75) Caravella, J., and Lugovskoy, A. (2010) Design of next-generation protein therapeutics. *Curr. Opin. Chem. Biol. 14*, 520−528.
(76) Hackel, B. J., Kapila, A., and Wittrup, K. D. (2008) Picomolar affinity fibronectin domains engineered utilizing loop length diversity, recursive mutagenesis, and loop shuffling. *J. Mol. Biol. 381*, 1238−1252.
(77) Zahnd, C., Kawe, M., Stumpp, M. T., de Pasquale, C., Tamaskovic, R., Nagy-Davidescu, G., Dreier, B., Schibli, R., Binz, H. K., Waibel, R., and Pluckthun, A. (2010) Efficient tumor targeting with high-affinity designed ankyrin repeat proteins: Effects of affinity and molecular size. *Cancer Res. 70*, 1595−1605.
(78) Henchey, L. K., Jochim, A. L., and Arora, P. S. (2008) Contemporary strategies for the stabilization of peptides in the α-helical conformation. *Curr. Opin. Chem. Biol. 12*, 692−697.
(79) Al-Shamkhani, A., Mallett, S., Brown, M. H., James, W., and Barclay, A. N. (1997) Protein Chemistry and Structure. *J. Biol. Chem. 272*, 5275−5282.
(80) Eldredge, J., Berkowitz, S., Corin, A. F., Day, E. S., Hayes, D., Meier, W., Strauch, K., Zafari, M., Tadi, M., and Farrington, G. K. (2006) Stoichiometry of LTβR Binding to LIGHT. *Biochemistry 45*, 10117−10128.
(81) Lamoureux, F., Picarda, G., Garrigue-Antar, L., Baud'huin, M., Trichet, V., Vidal, A., Miot-Noirault, E., Pitard, B., Heymann, D., and Rédini, F. (2009) Experimental Therapeutics, Molecular Targets, and Chemical Biology: Glycosaminoglycans as Potential Regulators of Osteoprotegerin Therapeutic Activity in Osteosarcoma. *Cancer Res. 69*, 526−536.
(82) Agematsu, K., Kobata, T., Sugita, K., Freeman, G. J., Beckmann, M. P., Schlossman, S. F., and Morimoto, C. (1994) Role of CD27 in T cell immune response. Analysis by recombinant soluble CD27. *J. Immunol. 153*, 1421−1429.